The formation of thick borders on an initially stationary fluid sheet

Museok Song[a)]
Hong Ik University, Chochiwon, Choong-Nam 339-701, Korea

Grétar Tryggvason
University of Michigan, Ann Arbor, Michigan 48109

(Received 9 November 1998; accepted 2 June 1999)

The formation of thick borders on an initially stationary two-dimensional fluid sheet surrounded by another fluid is examined by numerical simulations. The process is controlled by the density and the viscosity ratios, and the Ohnesorge number [$\mathrm{Oh}=\mu/(\rho d\sigma)^{0.5}$]. The main focus here is on the variation with Oh. The edge of the sheet is pulled back into the sheet due to the surface tension and a thick blob is formed at the edge. In the limits of high and low Oh, the receding speed of the edge is independent of Oh. Different scaling laws, however, apply for the different limits. The speed scales as $V\sim(\sigma/\rho d)^{0.5}$ in the low Oh limit as proposed by Taylor [Proc. R. Soc. London, Ser. A **253**, 13 (1959)] and as $V\sim\sigma/\mu$ in the high Oh limit. For low enough Oh, the edge forms a two-dimensional drop that is connected to the rest of the sheet by a thin neck and capillary waves propagate into the undisturbed sheet. The thickness of the neck reaches an approximately constant value that decreases with Oh, suggesting that the blob may ''pinch-off'' in the inviscid limit. [S1070-6631(99)04209-9]

I. INTRODUCTION

Atomization of liquids is an integral part of most combustion systems and many industrial processes (see Lefebvre,[1] for example). In many atomizers, as well as during natural processes that lead to the formation of drops, a thin sheet of liquid that eventually breaks up into drops is formed. The formation of such sheets is sometimes intentional, as in a simplex nozzle where swirl is used to produce a cylindrical cone, or it may form more naturally as in the late stages of drop breakup (Lefebvre[1]). While liquid sheets can disintegrate into droplets in many different ways, the initial breakup often consists of the edge receding and accumulating fluid. This particular scenario is clearly visible in a number of published pictures such as those in Mansour and Chigier,[2] and Rizk and Lefebvre.[3] While a large number of authors have examined the stability of liquid sheets (see, e.g., Mansour *et al.*,[2,4] Rangel and Sirignano,[5,6] Kawano *et al.*,[7] and Lozano *et al.*[8]) the focus has been on the formation and growth of waves that lead to a breakup in the middle of the sheet and not at the edge. It is, however, clear from the pictures referenced above that the actual formation of drops takes place at an edge, either at the rim of the sheet or at holes in the middle. The edges often eject filament that then break up into drops by capillary breakup (called ''rim disintegration'' by Fraser and Eisenklam[9]). The motion of a free edge of a liquid sheet was studied by Taylor,[10] who argued that the edge receded at the speed of an asymmetric wave. He also discussed the breakup of the edge, but did not identify conclusively the dominant mechanism. The breakup of filaments has been studied by a large number of authors (starting with Rayleigh[11]), but how such filaments are produced from the edge is not understood at the present time.

Here, we have a more modest objective and examine how a free two-dimensional edge recedes and accumulates fluid. The investigation is carried out by solving the unsteady Navier–Stokes equations numerically for an initially stationary sheet. The study shows that the edge of the sheet is pulled back by surface tension, forming a thick blob. The speed at which the edge is pulled back depends primarily on the Ohnesorge number and to a lesser degree on the density and viscosity ratio of the sheet and the surrounding fluid. For low enough Ohnesorge number, the edge forms a two-dimensional drop that is connected to the rest of the sheet by a thin neck. This ''necking'' is a purely two-dimensional effect that is quite different from the breakup of a circular fluid filament into drops. Although we examine an initially stationary sheet here, our study is motivated by simulation of the Kelvin–Helmholtz instability between immiscible liquids which show a two-dimensional pinch-off for finite density ratios and high Reynolds numbers (Tryggvason and Unverdi[12]). We note that two-dimensional ''pinching'' has also been seen in Hele–Shaw flows (Tryggvason and Aref[13]) and more recently in inviscid simulations of the Kelvin–Helmholtz instability between immiscible liquids of the same density (Hou, Lowengrub, and Shelly[14]). The downstream evolution of a fluid sheet emerging from a finite size slot is approximated by the time evolution of a two-dimensional sheet.

The motion of the edge of a liquid sheet has been examined analytically by Keller and Miksis,[15] who derived a similarity solution for the initial motion of a fluid wedge. Computational studies appear to be limited to the work of Oguz and Prosperett,[16] who conducted boundary integral simulations of the evolution of a thin sheet of air surrounded by

[a)]Electronic mail: msong@wow.hongik.ac.kr

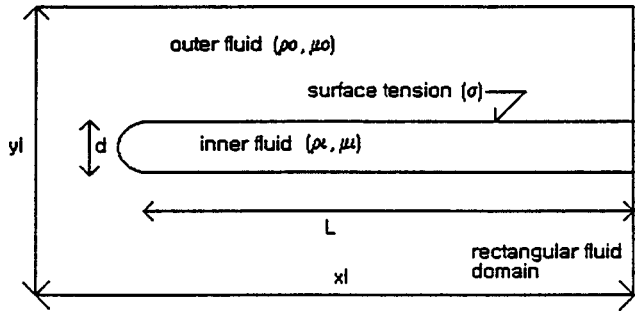

FIG. 1. Definition sketch of the problem.

liquid. Their study was motivated by the coalescence of a liquid drop with a flat surface and their primary focus was on the effect of the approach velocity of the drop.

In addition to quantifying the process, we offer an explanation of the dynamics of the neck formation by looking at both the vorticity and the pressure distribution. In the following sections the formulation of the problem with a brief explanation of the numerical procedure is given and the results, with discussions, follows.

II. FORMULATION AND NUMERICAL PROCEDURE

The initial setup of the problem is shown in Fig. 1. The two-dimensional fluid sheet has density and viscosity ρ_i and μ_i, respectively, while the density and viscosity of the surrounding fluid is ρ_o and μ_o, respectively. The surface tension, σ, is constant and the fluids are initially stationary. The free end of the sheet, on the left, has a semicircle shape with a radius that is equal to half the sheet thickness, d. The infinitely long sheet is modeled as a sheet of length L, so our simulation must be stopped before any disturbance reaches the right boundary.

The flow evolution is controlled by d and the material properties ρ_i, ρ_o, μ_i, μ_o, and σ. Simple dimensional reasoning yields three dimensionless parameters, the density ratio, $r=\rho_o/\rho_i$, the viscosity ratio, $m=\mu_o/\mu_i$, and the Ohnesorge number, $\mathrm{Oh}=\mu_i/(\rho_i d\sigma)^{0.5}$ (the ratio of viscous forces to surface tension). While different density and viscosity ratios can affect the flow we fix those at 0.1 in most of our investigation and focus primarily on the effect of Oh. For low enough density and viscosity ratios, the dynamics of the ambient fluid has a relatively minor effect as will be shown later.

The flow is governed by the Navier–Stokes equations that in conservative form are

$$\frac{\partial \rho \mathbf{u}}{\partial t}+\nabla\cdot(\rho\mathbf{u}\mathbf{u})=-\nabla p+\nabla\cdot\mu(\nabla\mathbf{u}+\nabla\mathbf{u}^T)+\int_f \sigma\kappa\mathbf{n}\delta(\mathbf{x}-\mathbf{x}_f)ds. \tag{1}$$

Here, $\mathbf{u}$ is the velocity, ρ is the density, μ is the dynamic viscosity, κ is the curvature of the interface, σ is the surface tension, and $\mathbf{x}_f$ is the position of the interface. $\mathbf{n}$ is a unit normal vector to the interface. Equation (1) is written for the whole flow field (both the sheet and the ambient fluid) and the surface tension at the interface is included as a delta function, which gives a contribution at the interface only. The density and viscosity are different for the sheet and the surrounding fluid, but we take the material properties of each fluid particle to remain constant, so

$$\frac{D\rho}{Dt}=0,\quad \frac{D\mu}{Dt}=0, \tag{2}$$

where D/Dt denotes the material derivative. This reduces the mass conservation equation to the incompressibility condition:

$$\nabla\cdot\mathbf{u}=0. \tag{3}$$

When combined with the momentum equation, Eq. (3) leads to a Poisson equation for the pressure.

Equations (1)–(3) are solved for the rectangular domain shown in Fig. 1. The top and bottom boundaries are taken as periodic and the vertical boundaries are full slip walls. To solve the Navier–Stokes equations a standard second-order, centered finite difference scheme with a multigrid Poisson equation solver for the pressure equation is used and the interface is updated using the front tracking method developed by Unverdi and Tryggvason.[17] This method introduces a separate grid for an interface moving across the stationary grid. At each time step, new density and viscosity fields on the stationary grid are obtained from the new location of the interface. Even though the interface has a finite thickness, it remains very sharp if fine stationary grids are used—the thickness of the interface is of the order of the mesh size of the stationary grid. This tracking method prevents numerical diffusion of the interface as well as numerical oscillations often encountered in high order shock capturing schemes. The surface tension, which is expressed as a delta function in Eq. (1), is distributed to the stationary grid following Peskin[18] and acts as a body force. The time integration is second order and the spatial resolution for the calculations presented here is 512×128 mesh points, in most cases. Resolution studies have shown that this grid results in an essentially fully grid-independent solution.

Although the fluid motion can be understood in terms of the pressure and the velocity, it is often helpful to examine the evolution of the vorticity in order to comprehend the kinematics of the flow better. The following equation governs the evolution of the vortex sheet strength of an interface separating two inviscid fluids of a different density:

$$\frac{d\gamma}{dt}+\gamma\frac{\partial\overline{\mathbf{U}}}{\partial s}\cdot\mathbf{s}=2A\overline{\mathbf{a}}\cdot\mathbf{s}-\frac{2}{\rho_i+\rho_o}\frac{\partial(p_i-p_o)}{\partial s}. \tag{4}$$

Here $\gamma=(\mathbf{u}_i-\mathbf{u}_o)\cdot\mathbf{s}$ is the vortex sheet strength at the interface, $\overline{\mathbf{U}}=0.5(\mathbf{u}_i+\mathbf{u}_o)$ is the velocity of a point on the interface moving with the average velocity, and $\overline{\mathbf{a}}=0.5(\mathbf{a}_i+\mathbf{a}_o)$ is the average of the fluid acceleration. The subscripts i and o denote conditions in the fluid on either side of the interface. $A=(\rho_o-\rho_i)/(\rho_o+\rho_i)$ is the Atwood ratio, p is the pressure, and $\mathbf{s}$ is a tangential vector to the interface. This equation was originally derived by Baker, Meiron, and Orszag[19] in a slightly different form, and has, for example, been used by Tryggvason[20] in his simulations of the Rayleigh–Taylor in-

stability, and by Rangel and Sirignano[6] for the Kelvin–Helmholtz instability. If we integrate Eq. (4) over a small material segment of the interface, Δs, and write the pressure jump across the interface as $p_o - p_i = \sigma\kappa$ where κ is the curvature, taken to be positive when the curvature center is in the fluid outside the sheet, we have the following equation for the change of the circulation of the segment:

$$\frac{d\Gamma(s)}{dt} = 2A \int_{\Delta s} \overline{\mathbf{a}}\cdot\mathbf{s}\, ds + \frac{2\sigma}{\rho_i + \rho_o}(\kappa_+ - \kappa_-). \tag{5}$$

Here κ_+ and κ_- are the curvatures of the interface at the boundaries of the segment. While the vorticity generated along the interface due to the curvature variation will diffuse into the fluid, the change in the circulation helps to explain the deformation of the interface.

III. RESULTS

In the following simulations the domain size is 4 by 1 in the x and the y directions, respectively, and the density and viscosity ratios are fixed at 0.1 unless otherwise stated. The initial length of the sheet is 3.7 and its thickness is 0.15 times the y dimension of the computational domain (see Fig. 1). As will be shown later the evolution is essentially inviscid for most practical systems and we have therefore selected to make time nondimensional by $(\rho_i^{0.5} d^{1.5}/\sigma^{0.5})$ in all the figures. Lengths are made dimensionless by d, the initial thickness of the sheet.

In Fig. 2(a) the interface separating the sheet from the ambient fluid is shown at 13 different dimensionless times starting from time zero. The Oh is 0.98 and we expect viscous effects to be large. For a better view, the lower parts of the interfaces are not plotted, except for the last time, and each frame is shifted slightly down and to the right with respect to the preceding one. The free end of the sheet is pulled to the right by the surface tension and Fig. 2(a) shows a monotonic increase in the size of the blob, formed at the edge, as it moves to the right. If we decrease the viscosity by a factor of 10 (Oh=0.098) the evolution of the boundary is different as shown in Fig. 2(b). As in Fig. 2(a), a growing rim moves to the right, gathering up fluid from the sheet, but unlike the high Oh case a neck forms in front of the blob. Lowering the Oh further (Oh=0.0098), Fig. 2(c), results in a more pronounced necking and the formation of symmetric waves that propagate along the sheet, away from the blob. For the lowest Oh, the wave has reached the end of the computational domain at the last few times. While the results are, in principle, not applicable to an infinitely long sheet for those times, we have included those frames since the rest of the solution appears to be relatively unaffected.

The observed evolution is perhaps best understood by examining the vorticity and the pressure. The vorticity and a few streamlines with respect to a stationary frame of reference are shown in Fig. 3(a) for the three cases from Fig. 2, at time 6.53. The vorticity is plotted in the upper half of each frame and the streamlines in the lower half. Only a part of the computational domain is shown, for clarity. Due to curvature variations, positive vorticity is generated near the end of the sheet, resulting in a dipole-like structure that pushes

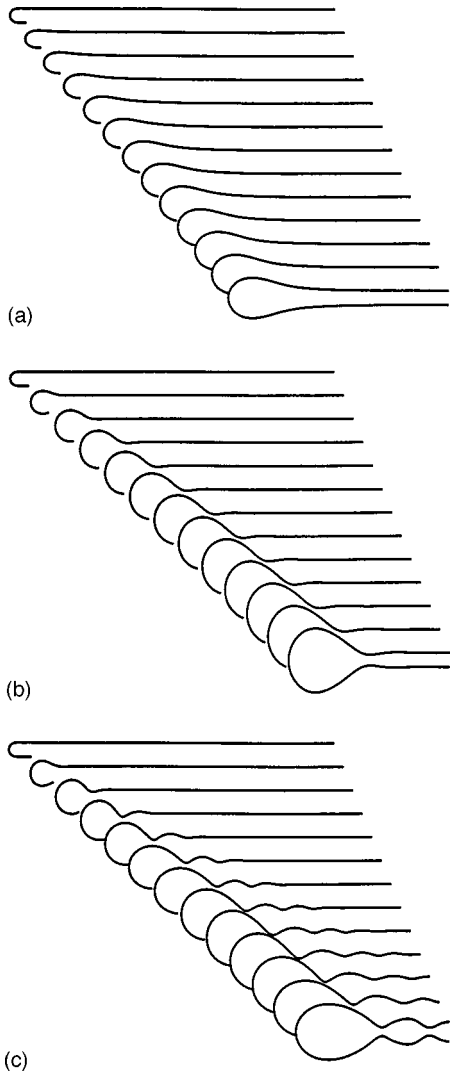

FIG. 2. Evolution of the sheet boundary. The lower part of the boundaries are not plotted except for the last time and each frame is shifted slightly down and to the right with respect to the preceding one. Dimensionless time increases from 0 to 13.08 by $\Delta t = 1.09$. (a) Oh=0.98, (b) Oh=0.098, and (c) Oh=0.0098.

the edge to the right. For the highest Oh (the top frame), this vorticity diffuses both into the sheet as well as into the ambient fluid, and even though there is a region of opposite curvature where the blob connects to the rest of the sheet, the vorticity generated there is overwhelmed by the diffusion of the primary vorticity. The absence of secondary vorticity is also clear in the streamline pattern. As the Oh is decreased (the middle frame), secondary vorticity of the opposite sign is generated due to the positive curvature in the neck region. The primary vorticity forms a boundary layer on the front part of the blob and is shed into the ambient fluid. The changes in the flow due to both the shed vorticity as well as the secondary vorticity are visible in the streamline plot. As the Oh is reduced further (the bottom frame), the boundary layer on the front of the blob becomes thinner and vorticity is also shed from the neck, into the blob. The small viscous diffusion allows the positive curvature to the right of the neck to form tertiary vorticity that causes secondary necking

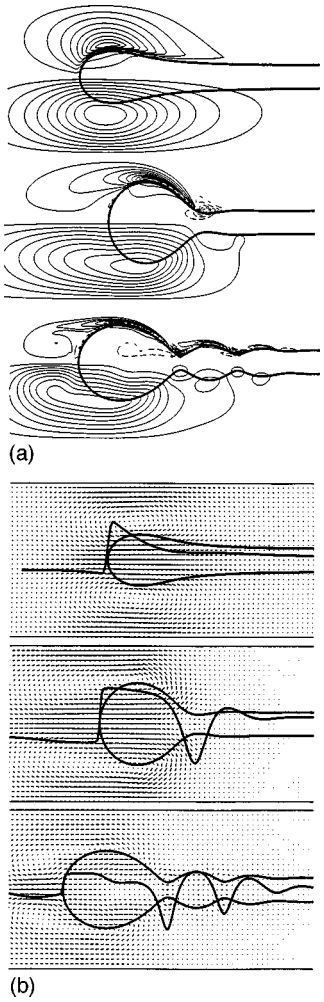

FIG. 3. Vorticity, stream function, velocity, and pressure distributions. Oh $=0.98$, 0.098, and 0.0098 from the top. Time$=6.53$. (a) Upper half: vorticity contours, dashed lines show negative vorticity. Lower half: stream function. (b) Velocity vector and pressure along the center line of the sheet.

and so on, leading to the formation of waves propagating to the right.

The velocity vectors and the pressure along the center line of the sheet are shown in Fig. 3(b) for the same cases as in Fig. 3(a). For the highest Oh case (the top frame), the pressure in the sheet is highest at the free edge and decreases as we move along the sheet to the right, accelerating the fluid to the right. Although the decrease in the pressure is nearly monotone, there is a slight increase as the forward motion of the fluid flowing from the blob is brought to a halt and deflected outward. Due to the finite size of the computational domain and the closed right and left boundary, there is a pressure drop in the ambient fluid between the two ends. In an infinitely large domain this would not be the case, although some local pressure drop would be necessary to move the ambient flow from the front of the blob to its back. Since the density of the ambient flow is relatively low, this effect has small influence on the sheet evolution (discussed later). As the effect of viscosity is reduced (the middle frame), the pressure in the blob is nearly constant and a region of very low pressure is seen in the neck where the blob is connected to the rest of the sheet. The fluid in the blob comes to a complete stop near the neck and a slight backflow is seen in the neck due to its propagation to the right. Further reduction in the Oh (the bottom frame) shows pressure fluctuations in the blob due to vorticity shed from the neck and several pressure minimums in the necks that have formed to the right of the blob. A slight backflow is seen in each neck.

The formation of the neck seen here is very different from necking of axisymmetric filaments (see Stone and Leal,[21] for example), where the azimuthal curvature creates a high pressure region in the neck which squeezes fluid away, further reducing the neck diameter. Here, there is a pressure minimum at the neck. The formation of the neck is easily explained by looking at the vorticity generated by the changes in curvature along the sheet surface. The secondary vorticity generated by the positive curvature where the blob joins the rest of the sheet pushes the blob boundary outward on the left, but inward on the right, thinning the sheet. Once the neck is formed, the negative curvature leads to vorticity of the same sign as the primary vorticity, forming a new blob connected to the rest of the sheet by a region of positive curvature. This process repeats itself, forming the wave train to the right of the blob. At high Oh, diffusion prevents the formation of any significant secondary vorticity and no neck forms. The increase in the relative velocity through the neck as it gets thinner and lowering the pressure is also consistent with inviscid analysis. We must therefore conclude that unlike axisymmetric necking, necking in two dimensions appears to be an essentially inviscid phenomena.

In Fig. 4(a) the position of the edge is plotted as a function of the nondimensional time for the three cases shown in Fig. 2. Initially, the motion is nearly linear, but at late time the speed is reduced slightly. This is, most likely, due to the finite size of the computational domain as will be discussed shortly. While the lower Oh sheets move faster than the high Oh sheet, there is very little difference between the two lower Oh cases. The diameter of the blob (measured perpendicular to the sheet at the point where it is thickest) for the same three cases, as well as the thickness of the ''neck'' for the two low Oh cases, is plotted versus nondimensional time in Fig. 4(b). Since the velocity of the edge is nearly linear, the diameter of the blob grows as a square root of time. As we saw for the speed of the edge, the high Oh blob grows slowest and the growth of the lower Oh blobs is comparable. The lowest Oh case, however, exhibits an oscillatory growth due to the waves propagating away from the neck. The neck forms relatively rapidly for both the low Oh sheets, but the lowest Oh sheet forms a considerably thinner neck (43% of the original thickness for Oh$=0.0098$ vs 73% for the Oh $=0.098$ case). As the blob diameter oscillates, so does the neck thickness.

The computations presented in Figs. 2–4 were done using a relatively small computational domain. To examine the influence of the domain size, we have recomputed the Oh $=0.098$ case using a twice as wide domain (resolved by a 512 by 256 grid), and the results are shown in Fig. 5. Both the original sheet from Fig. 2(b) as well as the results for the larger domain are shown at time$=6.53$ at the top. At the bottom the position of the edge, the size of the blob, and the size of the neck versus time are shown for both cases. The

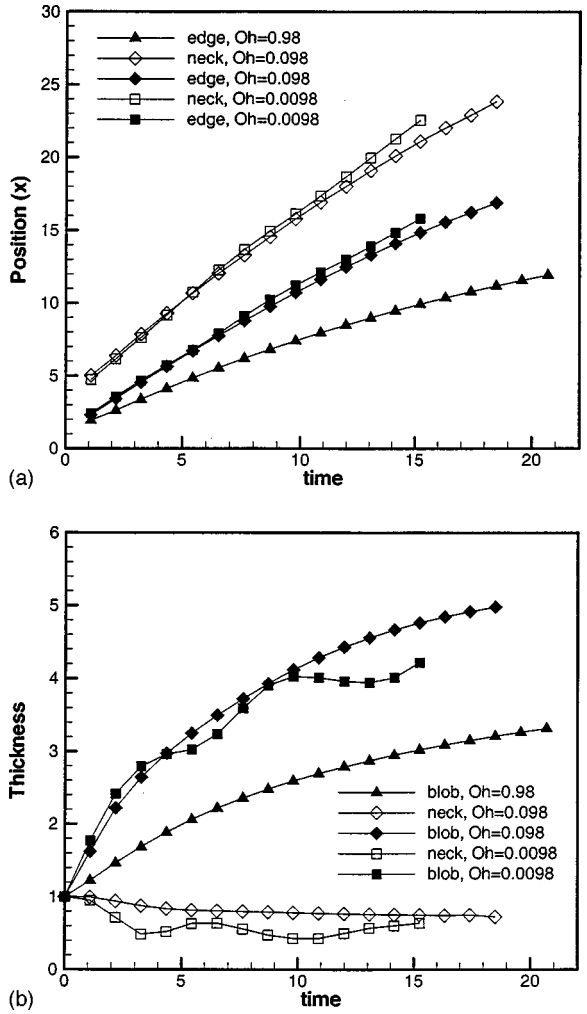

FIG. 4. (a) Edge and neck position vs time. (b) Blob and neck thickness vs time. Filled symbols represent the edge or the blob, and open symbols represent the neck. Squares are used for Oh=0.0098, diamonds for Oh =0.098, and triangles for Oh=0.98.

velocity of the edge in the larger domain is essentially constant (since the position changes linearly), but the velocity of the edge and the growth of the blob in the smaller domain is reduced slightly at later times. However, the initial behavior shows no significant dependency on the domain size, and this good agreement at early times suggests that the edge receding velocity can be estimated by measuring the slope of the line from the smaller domain at time 3 or so.

To examine the effect of the density and the viscosity ratio, we have repeated the Oh=0.098 simulation (using the smaller computational domain) for $r=m=0.01$ and $r=m=0.004$. The shape of the edge is essentially unchanged, but the evolution is slightly faster as seen in Fig. 6 where the position of the edge and thicknesses of the blob and the neck are plotted versus nondimensional time, along with the results for $r=m=0.1$ from Fig. 5. While the results for the larger density and viscosity ratio are essentially identical, the velocity of the edge for the higher ratios is about 12% lower. The neck thickness is, however, unchanged.

We have also examined the effect of the initial shape of the end of the sheet. Two half-ellipses with different eccentricities were used for the initial shape and the blob thickness and the edge position were compared with the results obtained using a half-circle end shape. The results were minimally affected by the initial shape of the end, in agreement with a similar test done by Oguz and Prosperetti[16] for a receding air film.

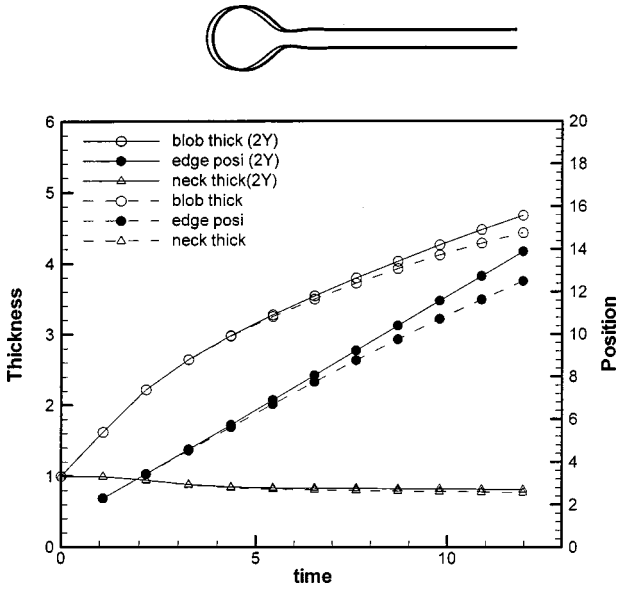

FIG. 5. Comparison of the interface shape and the evolution for different domain sizes. In the top frame, the thicker solid line is for the larger domain and the thinner solid line is for smaller domain at time=6.53. At the bottom, solid lines are for the bigger domain and dashed lines are for the smaller domain. Open circles: blob thickness. Filled circles: edge position. Triangles: neck thickness. Oh=0.098.

IV. DISCUSSION

For very viscous sheets (high Oh), the dynamics will be independent of the density. In this case there is no free parameter and the evolution must be independent of the Ohne-

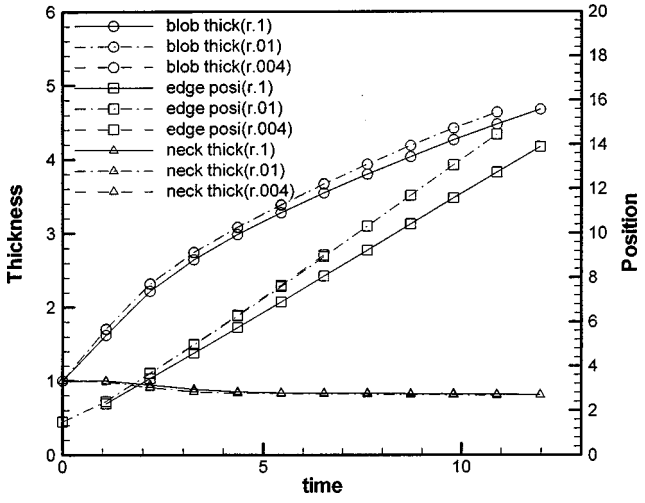

FIG. 6. Comparison of the interface shape and the evolution for different density and viscosity ratio. Solid lines: $\rho_o/\rho_i=\mu_o/\mu_i=0.1$, dashed/dot lines: $\rho_o/\rho_i=\mu_o/\mu_i=0.01$, dashed lines: $\rho_o/\rho_i=\mu_o/\mu_i=0.004$. Circles: blob thickness. Squares: position of the edge. Triangles: thickness of the neck. Oh=0.098.

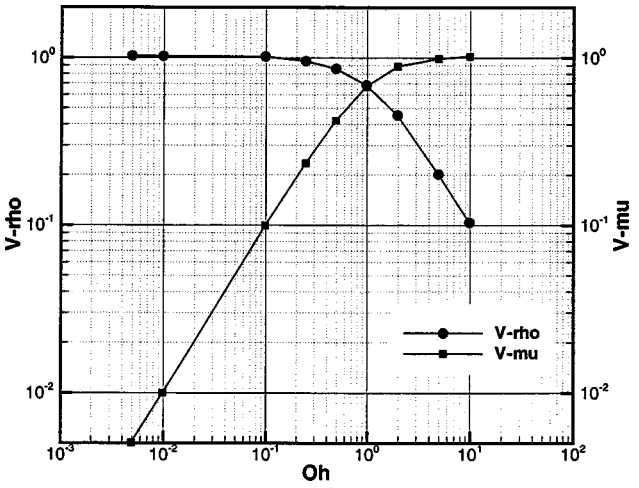

FIG. 7. Dimensionless edge translation speed. Circles are used for $V_\rho = V/(\sigma/\rho_i d)^{0.5}$ and squares for $V_\mu = V/(\sigma/\mu_i)$, where V is the dimensional edge speed.

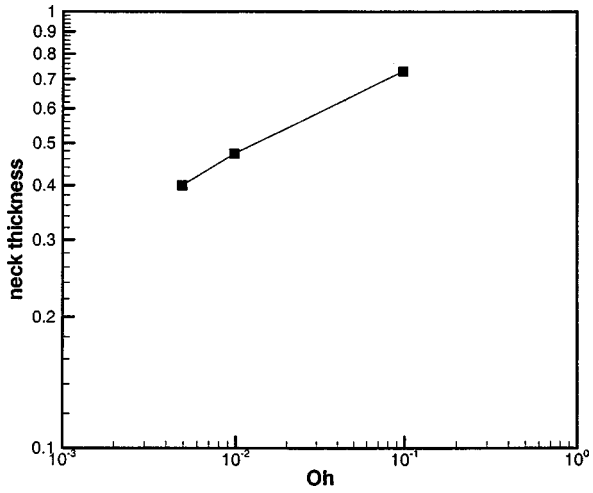

FIG. 8. Minimum neck thickness vs Oh.

sorge number. For nearly inviscid sheets (low Oh), the evolution is independent of the viscosity and since there is again no free parameter, the evolution must also be independent of the Ohnesorge number in this limit. The behavior is, of course, different and while the velocity must scale as $V \sim (\sigma/\rho d)^{0.5}$ in the low Oh limit, in the high Oh limit it must scale as $V \sim \sigma/\mu$. To examine where the transition takes place, we show the translation speed of the edge as a function of Oh in Fig. 7. The speed is estimated from Fig. 4(a), and similar plots from a few additional simulations, by computing the slope of the curve shortly after the initial acceleration has been completed. The results in Fig. 5 suggest that the velocity at this time is independent of the size of the computational domain and that it will remain constant in unbounded domains. The speed is made nondimensional in two ways, using the velocity scales defined above. For the low Oh range we see that $V = 1.02(\sigma/\rho_i d)^{0.5}$, independent of Oh, and for the high Oh, $V = 1.02(\sigma/\mu)$, again independent of Oh. Between those two limiting cases there is a transition region ($0.1 < \mathrm{Oh} < 5.0$) where the velocity depends on Oh.

The speed of the wave propagating in front of the blob can be computed by linear theory for a capillary wave on a thin sheet[22] In nondimensional units (velocity divided by $\sqrt{\sigma/\rho_i d}$), the phase speed and the group speed are given by

$$c = \sqrt{\frac{kd}{\rho_o/\rho_i + \coth(kd/2)}} \tag{6}$$

and

$$U = \frac{c}{2}\left(3 + \frac{(kd/2)\,\mathrm{csch}^2(kd/2)}{\rho_o/\rho_i + \coth(kd/2)}\right), \tag{7}$$

respectively. Here, k is the wave number defined as $k = 2\pi/\lambda$, where λ is the wavelength. For the lowest Oh, Eqs. (6) and (7) give dimensionless phase and group speeds of 1.443 and 2.419, respectively, using λ measured as the distance between the two wave crests next to the neck in Fig. 2(c) at time=6.53. The phase and group speeds measured directly from Fig. 2(c) are 1.43 and 2.41, respectively. The phase speed is found by tracing the location of the crest of the first wave for four consecutive times starting with time 6.53, and the group speed is found by tracing the first point where perturbations of the sheet are noticeable. Since the first wave to the right of the blob does not leave the blob, it follows that the edge must move with a speed that is only a little slower (since the blob is getting longer as it grows). Taylor[10] suggested that the receding speed of the edge should be $\sqrt{2} = 1.414$ using the same dimensionless unit as ours. The translation speed of the neck is very close to Taylor's (1.35 for Oh=0.098), but the speed of the edge itself is slightly different since the blob is getting bigger as it moves. For the initial transition this difference is a $t^{-1/2}$ correction and for the later time it is associated with the elongation of the bob as seen in Fig. 2. For the larger density and viscosity ratios the speeds of the edge and the neck are 1.21 and 1.55, respectively, for Oh=0.098 in the same dimensionless unit.

To examine how the thickness of the neck changes with Oh, the minimum thickness is plotted versus Oh in Fig. 8. No necking is observed for Oh higher than about 0.25. The minimum thickness of the neck obviously decreases with Oh and it seems fairly likely that the thickness would become zero if viscosity was totally absent. We note that a somewhat similar effect is seen for two bubbles rising side by side. Inviscid analysis shows that the bubbles move toward each other and will eventually touch, but if the Reynolds number is finite, the bubbles rise with a finite separation.

V. CONCLUSIONS

The formation of thick borders on an initially stationary two-dimensional fluid sheet, surrounded by another fluid is examined by numerical simulations. The primary controlling parameter is the Ohnesorge number (Oh). In the limits of high and low Oh, the speed at which the sheet recedes is independent of Oh, but different scaling laws apply for the different limits. Initially, the speed of the edge is about unity, in the proper nondimensional units. While the finite size of the domain used here leads to reduction in the edge velocity

as the blob grows, one simulation with a larger domain suggests that the velocity of a sheet in an unbounded fluid would remain constant.

The evolution is essentially inviscid for Oh<0.1. In terms of physical systems, this means that sheets of water thicker than 0.0014 mm and sheets of kerosene thicker than 0.016 mm, for example, can be treated as inviscid, at least as far as the speed of the edge is concerned. While very viscous sheets form a growing blob at their ends that gradually merges with the undisturbed part of the sheet, the blob at the edge of nearly inviscid sheets is connected to the rest of the sheet by a thin neck. The thickness of this neck reaches an approximately constant value that decreases with Oh, suggesting that the blob may ''pinch-off'' in the inviscid limit.

The original motivation for this study was the observation in Tryggvason and Unverdi[12] and Tauber, Unverdi, and Tryggvason[23] that a two-dimensional filament or a finger produced a blob as its end that appeared to pinch off in some cases. The problem studied here differs somewhat from the situation there since the sheet is initially stationary. The effect of acceleration or stretching on the breakup of the sheet remains to be explored. Some of the experimental figures referenced in Sec. I show that a nearly flat sheet with a thick rim ejects fingers of fluids that are perpendicular to the edge and break up into drops by capillary instability in a way very reminiscent of the ''crown'' formed when a drop impinges on a thin layer of liquid (Yarin *et al.*[24]). This seems to suggest that a straight (two-dimensional) edge is unstable to three-dimensional disturbances that are much longer than the thickness of the edge and that this instability eventually evolves into those fingers. An understanding of this process would greatly enhance the ability to predict drop sizes resulting from the breakup of a thin film.

ACKNOWLEDGMENTS

This work was supported in part by NASA Contract No. NAG3-2162. M.S. was partially supported by RIMSE of Seoul National University (98-7).

[1] A. H. Lefebvre, *Atomization and Sprays* (Taylor & Francis, London, 1989), pp. 1–34.
[2] A. Mansour and N. Chigier, ''Disintegration of liquid sheets,'' Phys. Fluids A **2**, 706 (1990).
[3] N. K. Rizk and A. H. Lefebvre, ''Influence of liquid film thickness on airblast atomization,'' Trans. ASME: J. Eng. Gas Turbines Power **102**, 706 (1980).
[4] A. Mansour and N. Chigier, ''Dynamic behavior of liquid sheets,'' Phys. Fluids A **3**, 2971 (1991).
[5] R. H. Rangel and W. A. Sirignano, ''Nonlinear growth of Kelvin–Helmholtz instability—Effect of surface-tension and density ratio,'' Phys. Fluids **31**, 1845 (1988).
[6] R. H. Rangel and W. A. Sirignano, ''The linear and nonlinear shear instability of a fluid sheet,'' Phys. Fluids A **3**, 2392 (1991).
[7] S. Kawano, H. Hashimoto, H. Togari, A. Ihara, T. Suzuki, and T. Harada, ''Deformation and breakup of an annular liquid sheet in a gas stream,'' Atomization Sprays **7**, 359 (1997).
[8] A. Lozano, A. Garcia-Olivares, and C. Dopazo, ''The instability growth leading to a liquid sheet breakup,'' Phys. Fluids **10**, 2188 (1998).
[9] R. P. Fraser and P. Eisenklam, ''Research into the performance of atomizers for liquids,'' Imp. Coll. Chem. Eng. Soc. J. **7**, 52 (1953).
[10] G. I. Taylor, ''The dynamics of thin sheets of fluid. III. Disintegration of fluid sheets,'' Proc. R. Soc. London, Ser. A **253**, 313 (1959).
[11] Lord J. W. S. Rayleigh, ''On the instability of jets,'' Proc. London Math. Soc. **10**, 4 (1878).
[12] G. Tryggvason and S. O. Unverdi, ''The shear breakup of an immiscible fluid interface,'' in *Proceedings of the C. S. Yih Memorial Symposium*, edited by W. Shyy (Cambridge University Press, Cambridge, 1999).
[13] G. Tryggvason and H. Aref, ''Numerical experiments on Hele–Shaw flow with a sharp interface,'' J. Fluid Mech. **136**, 1 (1983).
[14] T. Y. Hou, J. S. Lowengrub, and M. J. Shelley, ''The long-time motion of vortex sheets with surface tension,'' Phys. Fluids **9**, 1933 (1997).
[15] J. B. Keller and M. J. Miksis, ''Surface tension driven flows,'' SIAM (Soc. Ind. Appl. Math.) J. Appl. Math. **43**, 268 (1983).
[16] H. N. Oguz and A. Prosperetti, ''Surface-tension effects in the contact of liquid surfaces,'' J. Fluid Mech. **203**, 149 (1989).
[17] S. O. Unverdi and G. Tryggvason, ''A front tracking method for viscous incompressible flows,'' J. Comput. Phys. **100**, 25 (1992).
[18] C. S. Peskin and D. M. McQueen, ''A three-dimensional computational method for blood flow in the heart. I. Immersed elastic fibers in a viscous incompressible fluid,'' J. Comput. Phys. **81**, 372 (1989).
[19] G. R. Baker, D. I. Meiron, and S. A. Orszag, ''Vortex simulation of the Rayleigh–Taylor instability,'' Phys. Fluids **23**, 1485 (1980).
[20] G. Tryggvason, ''Numerical simulations of the Rayleigh–Taylor instability,'' J. Comput. Phys. **75**, 253 (1988).
[21] H. A. Stone and L. G. Leal, ''Relaxation and breakup of an initially extended drop in an otherwise quiescent fluid,'' J. Fluid Mech. **198**, 399 (1989).
[22] L. M. Milne-Thomson, *Theoretical Hydrodynamics* (MacMillan, London, 1968), pp. 442–449.
[23] W. Tauber, S. O. Unverdi, and G. Tryggvason, ''The non-linear behavior of a sheared immiscible fluid interface'' (unpublished).
[24] A. L. Yarin and D. A. Weiss, ''Impact of drops on solid-surfaces—Self-similar capillary waves and splashing as a new-type of kinematic discontinuity,'' J. Fluid Mech. **283**, 141 (1995).